

Stopping of multicharged ions in dense and fully ionized hydrogen

D. Gardes, A. Servajean, and B. Kubica

Institut de Physique Nucléaire, Boîte Postale 1, 91406 Orsay CEDEX, France

C. Fleurier and D. Hong

Groupe de Recherches sur l'Energétique des Milieux Ionisés, Université d'Orléans, 45067 Orleans, France

C. Deutsch and G. Maynard

Laboratoire de Physique des Gaz et des Plasmas, Université Paris-Sud,

Bâtiment 212, 91405 Orsay CEDEX, France

(Received 28 January 1992; revised manuscript received 19 May 1992)

Enhanced stopping and effective charges of energetic (C^{4+} , S^{7+} , and Br^{6+}) ions in dense plasmas are considered within the framework of the standard stopping model (SSM), the most economical extension to plasmas of the standard cold-matter formalism (Bohr-Bethe-Bloch). The main goal of this work is to check quantitatively the SSM predictions using the setup SPQR II (Stopping Plasma Quantitatively Reinforced) developed at Orsay. It consists of a dense hydrogen discharge inserted in an ion-beam line from a tandem Van de Graaff accelerator. Simultaneous ion spectrometry and plasma diagnostics yield quantitative energy-loss measurements, monitored by target free electrons. Specific aspects of the project such as, ion-beam-plasma interface, synchronization of plasma with beam time structure, and ion transmission in the target, are given due attention. Measured enhanced plasma stopping and projectile effective charge are then quantitatively matched with theoretical predictions, for ions with a kinetic energy between 1 and 2 MeV/amu. Relevance to heavy-ion-driven inertial compression is stressed.

PACS number(s): 52.40.Mj, 52.70.-m, 52.80.-s, 28.52.-s

I. INTRODUCTION

The interaction of ion beams with dense and fully ionized plasmas has been very recently promoted as a major domain of investigation [1–6]. It lies at the borderline of atomic and discharge physics. These topics are of a crucial significance in asserting the feasibility of manipulating intense beams of light or heavy ions toward the goal of compressing hollow microspheres (a few hundred microns in diameter) up to the ignition of the deuterium + tritium fuel delivering α particle and neutron thermonuclear yields.

The basic mechanisms underlying the physics of charged particles stopping in various states of matter have been the object of intense scrutiny since the very early days of quantum mechanics. For instance, the seminal 1913–15 Niels Bohr papers on the atomic model, are mostly dedicated to an impact-parameter formulation of ion stopping. Since then, the electromagnetic coupling between projectiles and target particles has always been the topic of ever increasingly sophisticated approaches. As a result, we now have a very large body of data for the stopping of ions in a neutral target.

However, all these studies were invariably conducted with an electrically neutral target material. Recently, the consideration of fully ionized targets, composed of ions and electrons, has emerged as a novel challenge with major concerns for thermonuclear research, high-energy particle acceleration, and related fields of interest. To mention just a few, heavy- and light-ion inertial fusion [1], particle heating of tokamak plasmas [1], and regen-

eration of free μ mesons in μ -catalyzed fusion [1] put increasing demands on the characterization of plasma targets and plasma lenses in various contexts. In all cases, the plasma-stopping capabilities for multicharged ions with energy in the MeV/amu range stand as a prerequisite to further progress in the above-mentioned fields of endeavor.

Many theoretical and numerical efforts [1–4,6] have already largely anticipated the specific features of the ion-target plasma interaction. According to these investigations, a consistent pattern of understanding has been produced.

Target electrons respond more efficiently to the projectile electric field when less bound in the target medium. Therefore, detached, free electrons are thus expected to provide the largest stopping effect. Moreover, excited but still bound electrons in a target should be more efficient than ground-state ones. These findings build up a concept of the so-called enhanced plasma stopping (EPS).

The predicted EPS arises from a few simple changes, entirely included in the most straightforward extension to a plasma target, of the well known (Bethe) cold-matter stopping expression. For partially ionized material, free electrons, bound electrons, and plasma ions contribute to energy loss. Ignoring relativistic corrections and the usually very small ion contribution, the stopping power dE/dx is given by

$$\frac{dE}{dx} = \frac{4\pi N_0 e^4 \rho}{A_T m_e V_1^2} Z_{\text{eff}}^2 [\bar{Z} \ln \Lambda_F + (Z_T - \bar{Z}) \ln \Lambda_B], \quad (1.1)$$

where $E = MV_1^2/2$, ρ is the density of the stopping medium, N_0 is Avogadro's number, e is the electron charge, m_e is the electron mass, Z_{eff} is the effective charge of beam ions, V_1 is the projectile velocity, A_T is the target atomic weight, Z_T is the target atomic number, \bar{Z} is the average ionization in target, and Λ_B, Λ_F are the arguments of the Coulomb logarithms for bound and free electrons, respectively.

For high target-electron velocities, Λ_B is given by the familiar Bethe expression

$$\Lambda_B = \frac{2m_e v_1^2}{I_{\text{av}}}, \quad (1.2)$$

where I_{av} is a geometric average of the effective excitation and ionization potential of the bound electrons. The expression for Λ_F is

$$\Lambda_F = \frac{2m_e v_1^2}{\hbar\omega_p}, \quad (1.3)$$

where ω_p is the plasma frequency. At low velocity, when one has $\Lambda_F < 1$, it must be modified.

Equation (1.1) implies the neglect of any collective stopping effect due to the high intensity of the ion beam, in agreement with recent investigations of the target corona instabilities [5]. Equation (1.1) is the high-temperature limit of more sophisticated estimates for the bound- and free-electron stopping power in the dense target plasma. Moreover, for partially stripped projectiles, an equally significant enhanced stopping also arises from the strongly reduced recombination [6] between incoming ion and free electrons. Such drastic behavior maintains a relatively high Z_{eff} , in contrast to that in cold matter, where the ion projectile can easily pick up bound electrons from target atoms (or ions) located near its trajectory. Thus the EPS physical content rests essentially on the much enhanced response of plasma free electrons, together with highly increased Z_{eff} values compared to nominally equivalent cold target, i.e., ones with the same line-integrated nuclear density (number/cm²). n_e is the free-electron density target and l the linear ion range within.

The present work aims at delivering a rather thorough discussion of EPS from every possible point of view: experimental, numerical, and theoretical. In Sec. II, numerological arguments are developed in order to pave the way for an original experimental program, elaborating on already existing facilities in nuclear as well as in plasma physics laboratories. The Bohr-Bethe-Bloch (BBB) stopping theory in cold matter based on Eq. (1.1) is given an extended framework for plasma stopping with the standard stopping model presented in Sec. III. Conditions expected for a hot target to check out EPS and other related effects are worked out in Sec. IV. The SPQR II (stopping plasma quantitatively reinforced) experimental setup, making use of the synchronized firing of a linear plasma column with an ion beam from a tandem Van de Graaf accelerator, is disclosed in Sec. V. A thorough discussion of beam and plasma diagnostics is also given there. Ion transmission through target plasma is given a detailed account in Sec. VI A.

Quantitative investigation of ion energy loss is reported in Sec. VI B. Comparison between experimental results and SSM predictions are also shown herein. Sec. VII summarizes methods and results.

II. A BIT OF NUMEROLOGY

All heavy-ion fusion (HIF) scenarios claim that current densities up to 10 kA/cm² are required to achieve a break-even [2–4]. Nevertheless, even under these unusual conditions, the average ion-ion distance in the beam remains much larger than the electron fluid screening lengths. These latter are deduced either from Debye-Hückel theory with

$$\lambda_D = (\text{cm}) = 6.90 \left[\frac{T(\text{K})}{n(\text{cm}^{-3})} \right]^{1/2}, \quad k_B T \gg \epsilon_F \quad (2.1)$$

and the Fermi energy

$$\epsilon_F = \frac{1.84}{r_s^2}, \quad r_s = \left[\frac{3}{4\pi n_e} \right]^{1/3} a_0^{-1} \quad (2.2)$$

or from the Thomas-Fermi expression (in units of a_0) $\sim (0.611r_s)^{1/2}$, at low enough temperature. These data always remain much smaller than the ion interparticle distances in the beams considered for HIF.

These simple considerations allow us to reduce the beam-target interaction to an ion-target one, by neglecting collective aspects in a first approach. In so doing, we have built the contents for the so-called reduction principle. This welcome simplification should nevertheless be taken with some reservations for the case of protons. The corresponding current densities may well range up to MA/cm², so that some caution should be exercised in every practical situation dealing with light ion beams.

With these minor restrictions taken into account, one is entitled to make use of conventional wisdom as to which intense beams are likely to appear dilute in the target. Had we considered intense electron beams, the collective phenomena would not have been so easily eliminated. For instance, potential wells can develop in the plasma produced by heating a thin foil, so that incoming projectiles are likely to be trapped and accelerated backward after several bouncing periods.

III. STANDARD STOPPING MODEL (SSM) [7,15]

A. General

The reduction principle advocated in Sec. II allows us to formulate the ion-beam-plasma interaction as that of a collection of independent charged particles. Therefore, we are led to reduce this interaction to ion stopping in the target. Previous studies have shown that to assess in a most economical way the suitability of Eq. (1.1) for describing plasma stopping, one has to up to a certain extent, stick to the guidelines given in Ref. [8].

These assumptions essentially sustain the validity range of the BBB formula (1.1) for the stopping of nonrelativistic point charges by isolated atom or cold matter, which

may be straightforwardly extended to hot and partially ionized material. Then, bound and free electrons, and also to a very limited extent plasma ions, contribute to the projectile stopping. We also limit our considerations to Λ_B [Eq. (1.2)] and Λ_F [Eq. (1.3)] larger than unity, which is well matched by experimental conditions discussed in the sequel.

B. Stopping-power formulation

Within the SSM framework, it is now straightforward to complete the stopping expression (1.1) with Barkas $\sim Z_{\text{eff}}^3$ and Bloch terms. In cold gas, those latter are no longer negligible when the Born parameter $Z_{\text{eff}}V_0/(V_1^2 + V_{\text{th}}^2)^{1/2}$ is comparable to 1. $V_0=1$ in atomic units. V_{th} is the thermal velocity of plasma electrons. Retaining also the very small target-ion contribution, one thus gets a more accurate stopping expression [7,8]

$$\frac{dE}{dx} = \frac{4\pi N_0 e^4 \rho Z_{\text{eff}}^2}{A_T m_e V_1^2} Z_T \left[\frac{\bar{Z}}{Z_T} L_0^F + \frac{Z_T - \bar{Z}}{Z_T} L_0^B + Z_{\text{eff}} \frac{V_0}{V_1} + Z_{\text{eff}}^2 \frac{V_0^2}{V_1^2} f(V_1^2) + \frac{m_e}{A_T} Z_T L_p \right], \quad (3.1)$$

with

$$L_0^F = Ln \frac{2m_e V_1^2}{\hbar \omega_p} - \frac{\langle V_{\text{th}}^2 \rangle}{V_1^2} - \frac{\langle V_{\text{th}}^4 \rangle}{2V_1^4} \quad (3.2)$$

and $\omega_p = \sqrt{4\pi e^2 n_e / m_e}$, the plasma frequency of the target free electrons.

$\langle V_{\text{th}}^2 \rangle$ is the usual average in terms of Fermi functions. $f(V_1^2)$ accounts for the standard Bloch correction, which bridges a gap between Bohr semiclassical expression and Bethe quantum-mechanical one. The last term $(m_e / A_T) Z_T L_p$ accounts for inelastic encounters between ion projectiles and target ions. It is non-negligible only for $V_1 \leq V_{\text{th}}$, or at very high plasma temperature.

The third term within brackets in the right-hand side (rhs) of Eq. (3.1) is the Barkas contribution $\sim Z_{\text{eff}}^3$. It per-

tains only to bound electrons and thus vanishes identically in a fully ionized target. In this case, the Born parameter becomes $Z_1 V_0 / V_1$.

Equation (1.1) and (3.1) share a same prefactor. For $V_1 \gg V_{\text{th}}$, $L_0^F \rightarrow \Lambda_F$ and $L_0^B \rightarrow \Lambda_B$. The relative importance of the four terms in the rhs of Eq. (3.1) is evaluated in Table I, for a target electron density of subsequent experimental interest. Obviously, the Barkas and Bloch corrections to the main Bethe contribution remain rather weak for all values of the Born parameter $Z_1 V_0 / V_1$.

C. Enhanced plasma stopping

According to Table I, Bethe-like stopping appears two or three times bigger in a fully ionized plasma than in the equivalent cold gas with the same density of electrons bound to atomic and molecular orbitals. A related EPS manifestation is reported on Fig. 1 for the penetration of a sulfur ion S^{6+} with a 2-MeV/amu kinetic energy in the hydrogen target; as a function of linear electron density in the target, the plasma energy deposition curve thus exhibits a pronounced maximum at the end of the trajectory, allowing for an intense and localized transfer of energy. Even more dramatic illustrations [18] are shown in Figs. 2–4, where we systematically compare for C^{n+} , Ar^{n+} , and U^{n+} the respective evolutions in cold gas and fully ionized hydrogen of Z_{eff} (left vertical axis) and energy loss (right vertical axis) in terms of penetration depth. A Monte Carlo code, making use of every excitation, ionization and recombination cross section, has been developed [8], together with a stopping calculation based on Eq. (3.1) to dynamically follow Z_{eff} in terms of projectile velocity V_1 . Obvious and dramatically different behavior appear by comparing plasma to equivalent (same linear density) cold-gas results. In three cases, one witnesses striking similarities. In cold gas, Z_{eff} data in terms of penetration range, and pertaining to several ionization stages, decay monotonically from initial value to a common cold-gas asymptotic limit [19] ($Z_1 =$ projectile atomic number),

TABLE I. Relative importance of Bloch and Barkas terms for cold-gas and plasma target. The target has a linear density of free electrons $n_e l = 1.5 \times 10^{19} \text{ cm}^{-2}$.

Ion	E (MeV/amu)	$\frac{Z_1 V_0}{V_1}$		Bethe		Barkas		Bloch	
		Gas	Plasma	Gas	Plasma	Gas	Plasma	Gas	Plasma
C^{4+}	2	0.56	0.62	5.63	12.48	0.08	0	-0.3	-0.35
S^{7+}	1	1.75	2.07	4.94	11.79	0.35	0	-1.16	-1.32
	1.5	1.43	1.69	5.34	12.2	0.23	0	-0.98	-1.13
	2	1.24	1.47	5.63	12.48	0.18	0	-0.85	-1.00
Br^{6+}	0.93	2.79	3.45	4.86	11.72	0.64	0	-1.61	-1.82

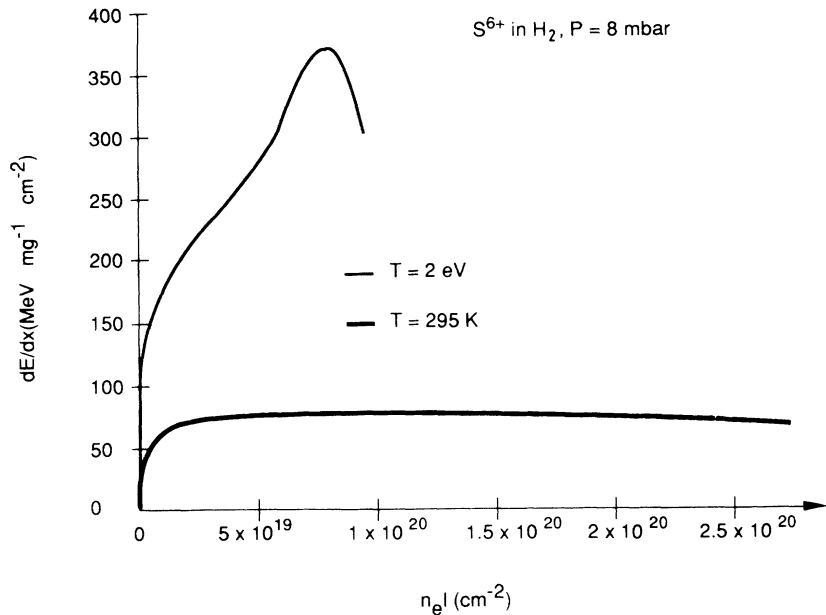


FIG. 1. Calculated stopping power dE/dx in terms of the linear electron density for S^{6+} with 2 MeV/amu stopped in the hot and fully ionized (upper curve) and cold (lower curve) hydrogen target.

$$Z_{\text{eff}} = Z_1 (1 - 1.034 \exp\{-[V_1 / (2.19 \times 10^8 \text{ cm/s})] Z_1^{-0.688}\}) \quad (3.3)$$

In contradistinction, Z_{eff} plasmas rise steadily. For the lightest carbon element, all ionization stages end up in C^{6+} for a maximum range corresponding to the experimental SPQR II setup detailed below. This effect increases with Z_1 . As a rule, projectile effective charges in plasma lie much higher [6] than their cold-gas homologous, except very near the end range, where a type of ca-

tastrophic recombination takes place. As a consequence, stopping powers $\sim Z_{\text{eff}}^2$ may increase by orders of magnitude. These specific Z_{eff} behaviors in plasma are essentially due to a quasihindered recombination between ion

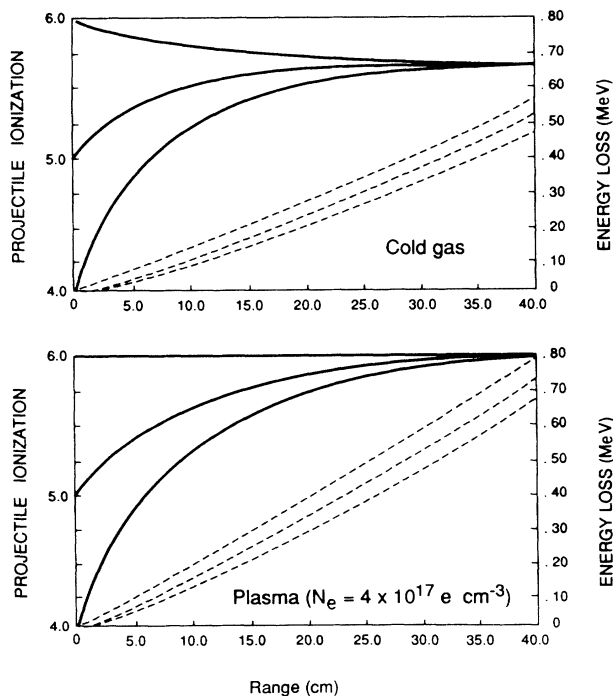


FIG. 2. Effective charges and energy losses of energetic C^{n+} ions with 2 MeV/amu in cold gas and fully ionized hydrogen.

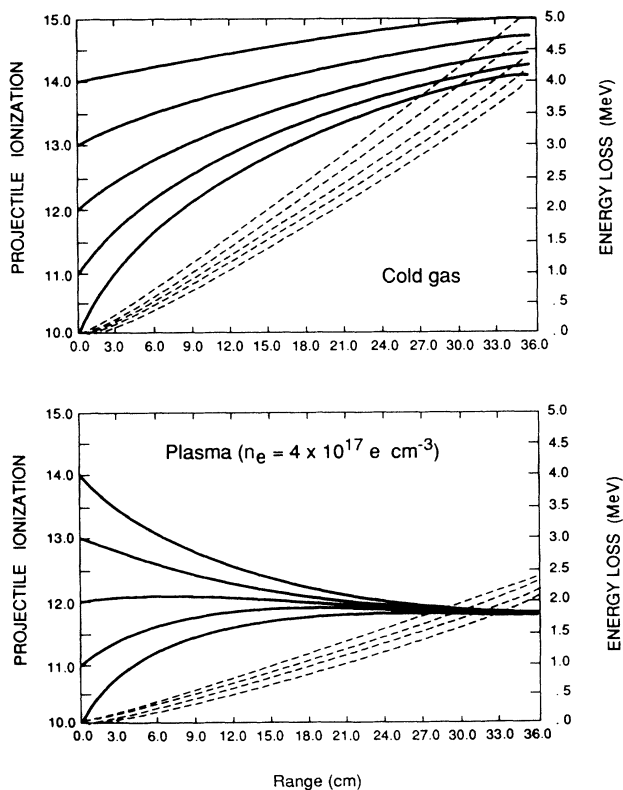


FIG. 3. Effective charges and energy losses of energetic Ar^{n+} ions with 1.4 MeV/amu in cold gas and fully ionized hydrogen.

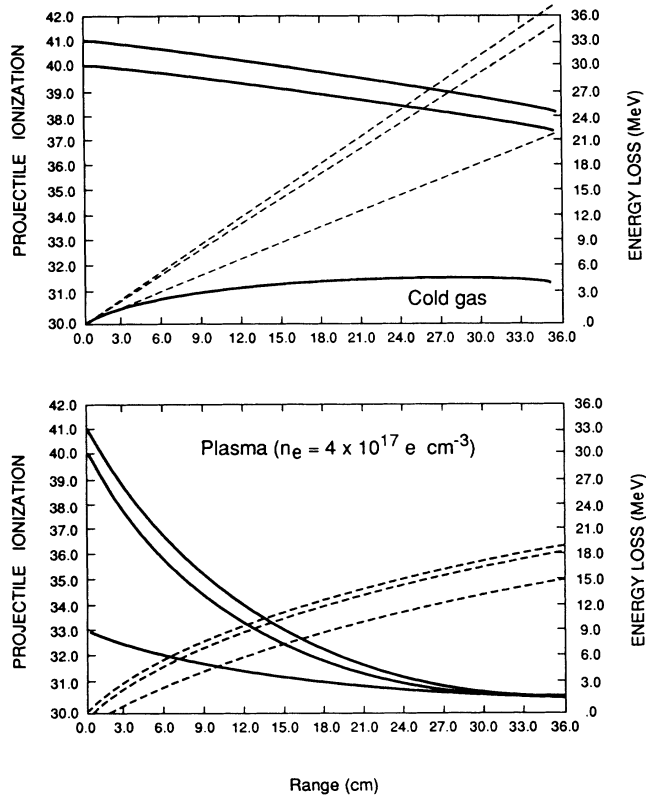


FIG. 4. Effective charges and energy losses of energetic U^{n+} ions with 1.4 MeV/amu in cold gas a fully ionized hydrogen.

projectile and target electron. The latter has a type of plane-wave behavior that prevents it from being used as a bound orbital. In cold gas, all electron states are bound ones.

Therefore, projectile recombination is made possible by transferring to it a bound electron instead of a target ion. As far as experimental verification of these predictions is concerned, target ionization looks like a much more significant parameter than temperature. We thus expect to witness these Z_{eff} plasma behaviors, even at a rather modest target temperature, a few eV, provided the target remains fully ionized.

IV. PRINCIPLES OF ION-BEAM-PLASMA EXPERIMENTS

A. General

The previous line of reasoning suggests a clear path to an experimental verification of above previsions. The reduction principle stated in Sec. II may be implemented to test EPS results (Sec. III). One thus feels entitled to replace a complex interaction of intense ion beams with a given target by that of a dilute beam out of a standard accelerating structure. The plasma target may thus be fired independently of the ion beam, provided the discharge ignition is synchronized with the beam time structure. In this fashion, it appears feasible to emulate a dense, plas-

ma produced, say, by a space-charge-dominated ion beam of inertial-confinement fusion (ICF) interest.

Such an approach builds up a backbone for the so-called SPQR II project started at Orsay. One can thus make use of standard accelerating structures delivering dilute pulses of ions in any charge state with any requested kinetic energy. One is left with a practical task of simultaneously performing beam spectrometry and plasma diagnostics. Before going on further, it is appropriate to derive a most useful scaling rule [7],

$$\frac{\Delta E}{E} = \frac{n_e l}{E^2}, \quad (4.1)$$

from Eqs. (1.1) and (3.1) between maximum energy loss and linear density of target electrons. l denotes penetration depth. Equation (4.1) allows us to match projectile energy with target-free-electron density. For a given $n_e l$, only a narrow range of E values will provide the largest stopping powers.

B. Parameter range

The SSM conditions (Table II) imply $V_1 \gg V_{\text{th}}$ with

$$V_1 (\text{cm/nsec}) = 1.39 \sqrt{E/M (\text{MeV/amu})}, \quad (4.2)$$

and

$$V_{\text{th}} (\text{cm/nsec}) = 5.9 \times 10^7 \sqrt{k_B T (\text{eV})}. \quad (4.3)$$

For a standard target temperature ~ 4 eV, $V_{\text{th}} \sim 0.12$ cm/nsec, while projectiles with a typical MeV/nucleon energy have $V_1 \sim 2$ cm/nsec. Therefore, $V_1 \gg V_{\text{th}}$ is easily fulfilled. One also easily checks that the ion-ion intra-beam distance remains on average much superior to the electron screening length in the target.

Let us pick up beam conditions considered below, with an intensity $I_0 = 500$ nA pulsed with a frequency $\nu = 1.25$ MHz (i.e., a pulse every 800 nsec). The number N_0 of ions within a micropulse is thus

$$N_0 = \frac{I_0}{veZ_1} = 5 \times 10^{12} \frac{I_0}{Z_1} \text{ ion/pulse}. \quad (4.4)$$

For a typical sulfur ion S^{7+} , this yields $N_0 = 3.6 \times 10^5$ ions/pulse. A micropulse lasts for $\tau = 2$ nsec. With a beam energy $E = 64$ MeV, the projectile ion's density is $n_0 \simeq 10^6 - 10^7$ cm $^{-3}$, in a volume containing pulse particles. The interprojectile distance thus is written as $d_0 = (4\pi n_0/3)^{-1/3}$ cm, which gives $d_0 \sim 1.3 \times 10^6 - 6 \times 10^5$ Å, much larger than the target classical screening length (2.1). For a plasma temperature ≥ 2 eV and Fermi energy

$$\varepsilon_F = 1.84 \left[\frac{4\pi r_e}{3} \right]^{2/3} a_0^2 < 2 \times 10^{-4} \text{ eV},$$

the condition $k_B T \gg \varepsilon_F$ is well fulfilled. a_0 denotes the Bohr radius. The corresponding and practically achievable λ_D values are plotted in Table II. They are at least three orders of magnitude below the considered d_0 values. Consequently the reduction principle is fully

TABLE II. Debye screening length (in Å) for a fully ionized hydrogen plasma with electron number density n_e and temperature T_e .

n_e (cm ⁻³) \ T_e	1	2	3	4	5
10 ¹⁵	2350.5	3324.2	4071.3	4701.1	5256
10 ¹⁶	743.3	1051.2	1287.5	1486.6	1662.1
10 ¹⁷	235	332.4	407.1	470.1	525.6
10 ¹⁸	74.3	105.1	128.7	148.7	166.2
10 ¹⁹	23.5	33.2	40.7	47	52.6
10 ²⁰	7.4	10.5	12.9	14.9	16.6

justified in this case. In order to validate the present SSM benchmark, we need a strongly ionized target. The simplest one is hydrogen. The corresponding Saha distribution of protons n_i and atoms n_n is written as

$$\frac{n_i}{n_i + n_n} = 2.4 \times 10^{21} \frac{T^{3/2}}{n_i} e^{-U_i/k_B T}, \quad (4.5)$$

in terms of ionization energy U_i . Ionization percentages are graphed in Fig. 5 for several pressures, as a function of plasma temperature. Above 2 eV, ionization is larger than 80%. The remaining hydrogen bound states are also in thermal equilibrium with free ones, which justifies, *a posteriori*, using the Saha distribution.

C. Beam-plasma energy transfer

To secure meaningful energy-loss measurements, one should request that ion stopping not perturb the plasma thermodynamics. To check up on this point, we compare the expected projectile energy losses to the energy content in the plasma target. We show the beam-plasma energy transfer is indeed negligible. The argument runs as follows.

According to above calculations, one expects that the

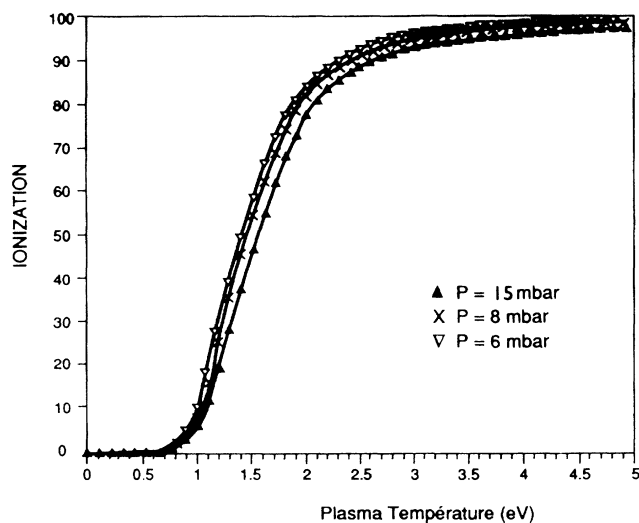


FIG. 5. Ionization rate (in %) in hydrogen plasma target as a function of temperature at three pressures.

considered ion beam, with an average width of ~ 0.3 cm, loses 10% of its kinetic energy in a plasma volume $\pi(0.15)^2 40$ cm³. This results in a overall 36- μ J energy loss in 2.83 cm³. Those estimates pertain to the setup detailed below in Sec. V, which can accommodate 100 ion micropulses for one plasma shot.

Selecting routine plasma parameters, i.e., $n_e = 5 \times 10^{17}$ cm⁻³, $T_e = 20$ 000 K, one gets

$$\frac{3}{2}(n_e + n_i)k_B T = (1.5 \times 10^{18})(1.73)(1.6 \times 10^{-19}) \text{ J cm}^3 \quad (4.6)$$

in volume $V \sim 2.83$ cm³.

The plasma volume interacting with the ion beam thus has a 1.19-J stored energy five orders of magnitude above the projectile energy loss (36 μ J). Moreover, this tiny amount of delivered energy is rapidly thermalized within the target through a very high electron-electron collision frequency,

$$\nu_{ee} = 2.9 \times 10^{-6} [n_e (\text{cm}^{-3})] \lambda_{ee} [T_e^{-3/2} (\text{eV})] \text{ sec}^{-1}, \quad (4.7)$$

with Coulomb logarithm

$$\lambda_{ee} = 23 - \ln [n_e^{1/2} (\text{cm}^{-3})] [T_e^{-3/2} (\text{eV})].$$

Here, we thus obtain

$$\lambda_{ee} = 3.44, \quad \nu_{ee} = 2.2 \times 10^{12} \text{ Hz}.$$

V. EXPERIMENTAL SETUP

A. Layout

An experimental realization of the above scheme for the interaction of ion beams with strongly ionized hydrogen plasma is achieved by Ohmic heating of a low-pressure hydrogen column. The gas is confined in an alumina tube and inserted on a beam line from a tandem Van de Graaff [9,10,13,16,17] (see Fig. 6). The plasma results from the powerful discharge of the capacitor bank delivering 5 kJ when operated at 15 kV. Special coupling ports have been developed [14] to insure the connection between the plasma target and the vacuum of the beam line. They consist of two fast valves associated with a differential pumping system. They are only opened during the plasma ignition and they reduce significantly the amount of cold gas at both sides of the plasma tube dur-

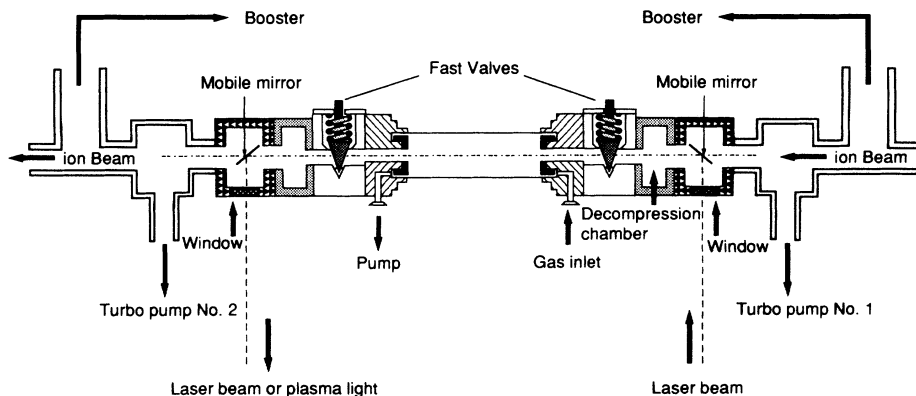


FIG. 6. Experimental setup. A linear plasma column is confined in an alumina tube connected to the beam line with two fast valves. Plasma diagnostics are realized using a laser beam injected during the plasma shot via two removable mirror systems.

ing the energy loss measurement. A variant of this setup devoted to plasma stopping of projectiles that are heavier than Ar has already been presented [11,12].

The energy loss of the heavy ions was performed using capacitive phase probes, which deliver an accurate timing signal that corresponds to the beam burst flowing through the detector. The energy-loss measurement results from a time-of-flight (TOF) comparison of the ions before and after interaction with the plasma. Figure 7 presents a schematic drawing of the phase-probe arrangement. A typical timing signal is presented in the same figure. An interesting property of this phase-probe detector is that it delivers signals in which the amplitude is proportional to the quantity of charge inside the beam burst. This information is essential in order to follow the

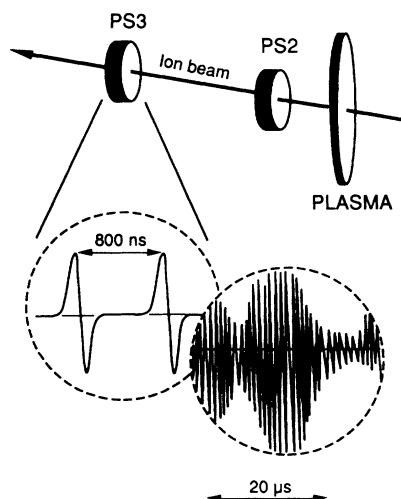


FIG. 7. Schematic presentation of the time-of-flight measurement. Each beam burst separated by 800 nsec delivers an electrical signal whose amplitude is proportional to the beam peak intensity. Two capacitive phase probes labeled PS2 and PS3 are used as start and stop detectors, respectively. A compressed time scale (i.e., 20 μ sec in the figure) shows the evolution of the transmitted intensity as a function of time during the plasma discharge.

evolution of the beam transmission during the plasma firing.

B. Operation

The ion beam has a time microstructure lasting 2 nsec repeated every 800 nsec. The plasma lifetime corresponds to about 100 μ s and it can be fired every 2 min.

200 μ sec after the opening of the fast valves, a time coincidence between the plasma light and a beam pulse starts the computer-aided measurement-and-control (CAMAC) acquisition system. Time signals delivered by the phase probes are then sequentially registered using a time-digital-converter multistop. The visualization of the time spectrum, and its memory storage are devoted to a special microprocessor controlled with a personal computer. Two Faraday cages enclose the plasma target and the data-acquisition equipment. They insure a shielding from the rf noise generated by the plasma discharge.

C. Diagnostics

Plasma diagnostics has to be synchronized with spectrometric measurements. Practice shows that on-line and off-line diagnostics do not differ by more than 5%. This allows us to proceed in two steps: a careful off-line diagnostic of the discharge, and a monitoring based on the light emission of the plasma during the experiment.

Several spectroscopic techniques are used independently to determine the temperature and the density of the plasma target [17]. Laser absorption at two different wavelengths, laser interferometry, and emission spectroscopy using the Stark broadening of the hydrogenic H_{β} line.

Results for the time evolution of electron density, temperature, and ionization are given in Figs. 8(a)–8(c) as a function of time, for several discharge voltages. The results reported are averages over several plasma shots. As expected, ionization is the highest at highest discharge voltage. The density of residual neutral atoms provides spectroscopic diagnostics through the hydrogen H_{β} line.

ΔE measurements are expected to be rather accurate in view of nearly constant temperature and ionization during a whole discharge lifetime. On other hand, one expects a strong time modulation of stopping quantities, following closely the density one.

VI. ION STOPPING IN DENSE PLASMA

A. Transmission

One may reasonably wonder whether the tiny ion beam considered above (Sec. IV C) will be able to make its way through the discharge from the entrance to the exit holes (3 mm in diameter). It could be easily deflected, as a simple calculation shows, by a steady 100-G magnetic field applied transversely to the beam. This could already result in a 1-mm transverse deviation at the discharge end [18]. Moreover, it is obvious that transient instabilities

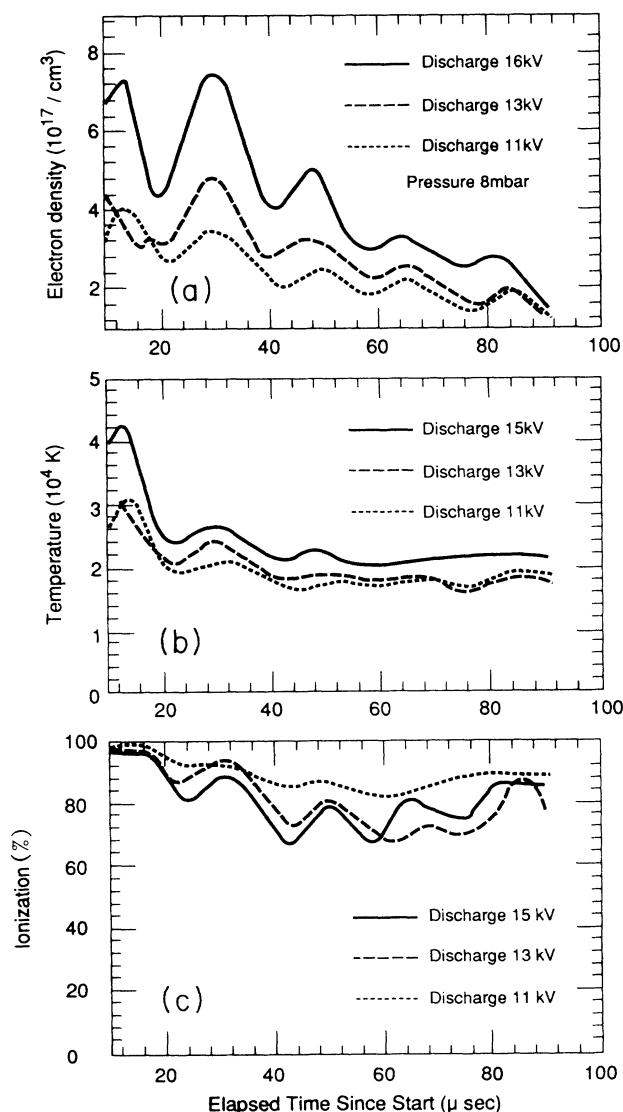


FIG. 8. Variation with time of discharge parameters for three charging voltages: (a) free-electron density, (b) temperature, (c) ionization.

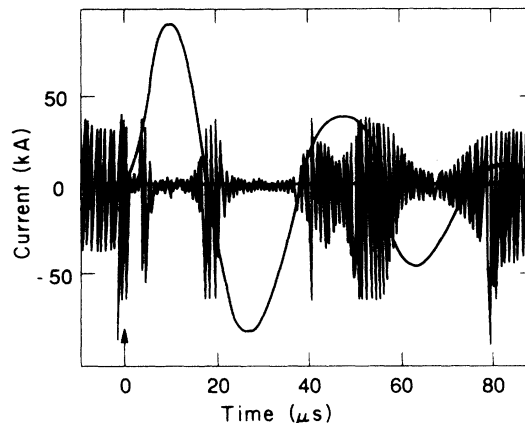


FIG. 9. Superposition of discharge current (solid line) to plasma transmission figures (15 kV).

may produce much larger fields with any orientation.

However, it is surely a tribute to the robustness of the present setup (Fig. 6) that the beam-plasma interaction remains axially symmetric. The ion beam always flows from the entrance to the exit hole during a complete plasma lifetime. This is evidenced by transmission figures [16] given in Fig. 9. From left to right, one first witnesses a deterministic noise arising from the discharge ignition, then a short (a few μsec) burst of plasma turbulence appears. Further on, one gets a nearly constant ion transmission followed by a kind of plasma lens effect. This latter has also been substantially confirmed and documented elsewhere [10]. These strong modulations of transmission are essentially monitored by the discharge current. They are shown superimposed on the transmission, Fig. 9.

B. Energy-loss measurements

Measured stopping quantities can now be compared to their theoretical SSM counterparts (Sec. III). At this point, it is convenient to recall that plasma stopping has to be referenced to cold-gas stopping with the same density of recombined electrons. This fictitious cold-gas equivalent is the true plasma reference. There is no initial cold-gas fill preceding the plasma ignition.

Our numerical codes based on the SSM carefully include the residual bound-electron contribution to discharge stopping. Therefore, a meaningful theory-experiment confrontation is likely to occur.

As expected from Sec. V C, measured ΔE follows closely the n_e time profile. This is confirmed in Fig. 10, where S^{6+} stopping with 1 MeV/amu initial energy is contrasted to n_e . As far as accuracy is concerned, it should be disclosed that uncertainty on time-of-flight measurements only amounts to ± 0.5 nsec. A larger fluctuation persists from shot to shot. Maximum rates for these fluctuations are respectively 18% and 12% for 15- and 13-kV ignition voltage.

They are responsible for a partial reproducibility of plasma conditions. A theory-experiment comparison is shown in Fig. 11. Experimental data have been measured

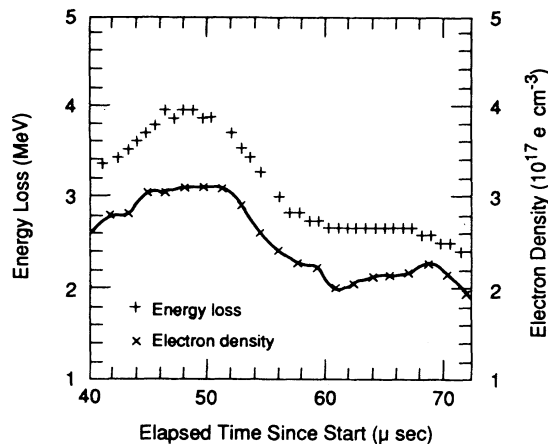


FIG. 10. Comparison of the stopping of sulfur ions (1 MeV/amu) with the evolution of the plasma electron density (solid line) as a function of time.

in a preliminary version of the experimental device, without the use of fast valves.

Energy losses of sulfur ions (2 MeV/amu) are compared with SSM calculations including the hypothesis of a constant $14+$ charge for the incident ion. Therefore, a certain amount of cold gas has contributed to the lifting up somewhat of the apparent plasma stopping for times greater than $50 \mu\text{sec}$. Shorter time measurements are in excellent agreement with theoretical profiles interpolated between those with $Z_{\text{eff}} \approx \text{const}$. The crucial V_1 -dependent parameter Z_{eff} is measured by firing a fully stripped C^{6+} reference beam at the same velocity as the considered one.

As far as the projectile state evolution is concerned, Fig. 12 provides a confirmation of the reliability of Eq. (3.1). It displays, for a given projectile energy, the stopping-power ratio (SPR) of two incoming ions with different charge states. The instantaneous, inflight, ion-

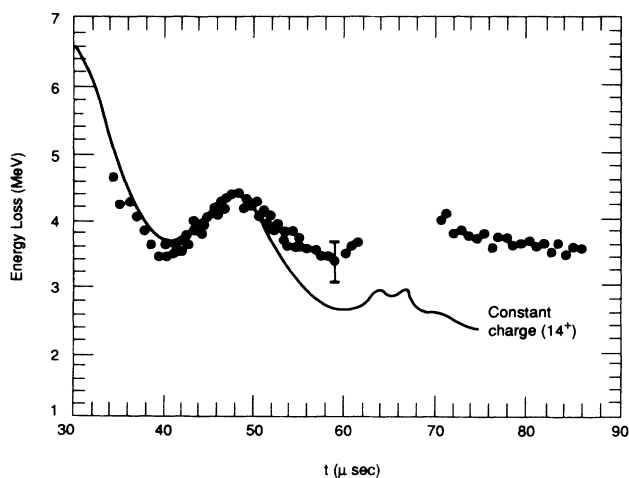


FIG. 11. Experimental energy losses (solid points) measured without fast valves, compared with the SSM prediction for S^{14+} with 2 MeV/amu in hydrogen plasma.

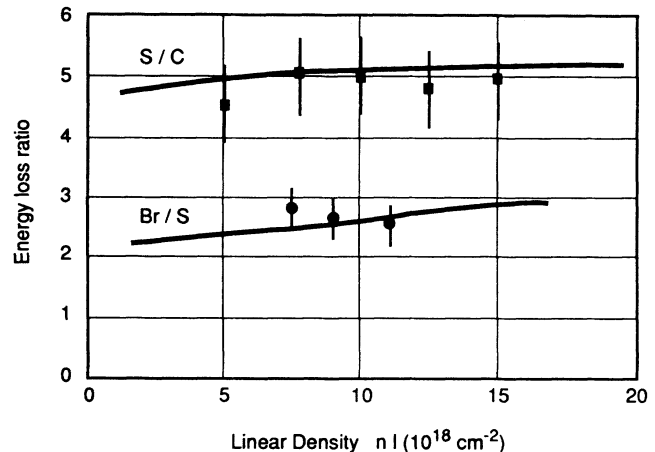


FIG. 12. Energy-loss ratio as a function of plasma linear density for carbon-sulfur ions and bromide-sulfur ions at the same velocity, compared with the ratio of the corresponding calculated effective charge (solid line). Initial projectile kinetic energy is 2 MeV/amu. The target is fully ionized hydrogen with $k_B T \approx 2.5 \text{ eV}$.

ization balance of the projectile, at a given velocity, is accurately followed by a detailed numerical one, including all the available channels for collisional ionization and recombination [9]. Measured SPR data are in very close agreement with those pertaining to the entrance projectiles effective charge $(13/5.9)^2 \approx 5$. This corresponds to S^{7+} and C^{4+} projectiles, with a 2-MeV/amu initial kinetic energy. Carbon ions get rapidly fully stripped within the plasma target, while sulfur charge states stabilize around S^{13+} . The horizontal line in Fig. 12 is deduced from a complete calculation with the above-mentioned numerical code. It matches very nicely the measured SPR data.

Another theory-experiment comparison is given in the same figure for sulfur and bromide ions in hydrogen plasma. Figure 13 summarizes the SSM calculations compared with experimental results. A quasilinear variation that has already been observed for heavier elements is then confirmed. Corresponding EPS values may be larger than 3, in some cases.

Data on the stopping of C^{4+} , S^{7+} , and Br^{6+} ions in the initial energy range 0.7–4 MeV/amu are of considerable interest for the final stopping phase, near the end of range, for particle-driven inertial fusion. Those data could provide a deeper insight into ion-beam transport in the reactor chamber containing the pellet, as well as into the beam-target compression process envisioned within the so-called classical energy deposition scenario. Within the SSM, our measurements may be extrapolated to other ion species through the scaling relationship

$$\frac{dE'}{dx}(Z', M', E') = \left(\frac{Z'}{Z} \right)^2 \frac{dE}{dx}(Z, M, M/M'E'), \quad (6.1)$$

for two ion projectiles with charge, mass, and kinetic energy (Z, M, E) and (Z', M', E') , respectively.

Results shown in Fig. 13 definitively confirm the con-

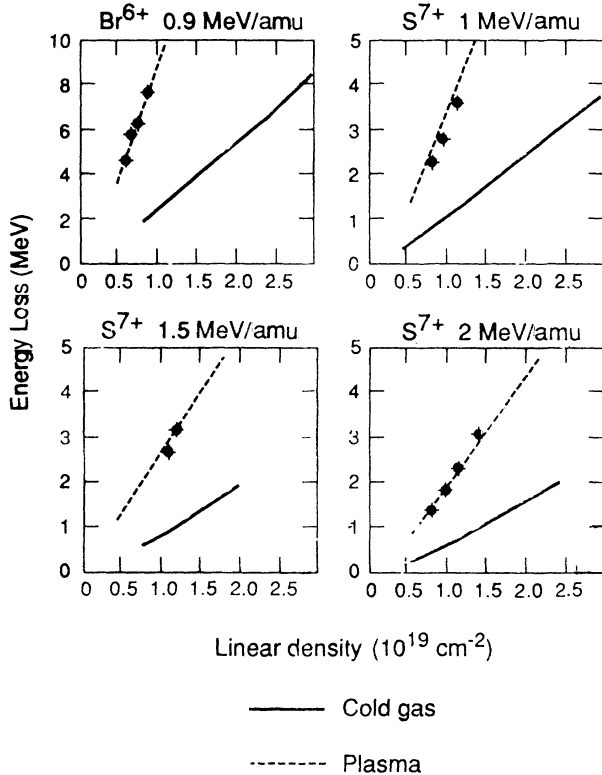


FIG. 13. Energy losses as a function of free plus bound-electron density in a hydrogen plasma for Br^{6+} with 0.93 MeV/amu and also S^{7+} with 1, 1.5, and 2 MeV/amu, respectively.

spicuous and strongly enhanced plasma stopping in a fully ionized hydrogen target, at several inertial projectile energies. It should be appreciated that a previous attempt using intense D^+ beams by Young *et al.* [1] has anticipated some of our findings about EPS in the field of light-ion-driven (ICF). Another important feature, in full agreement with Eq. (3.1), is the rather weak electron temperature dependence of the ion energy loss, provided the plasma ionization is kept constant. These facts allow us to produce stopping data of interest for inertial thermonuclear fusion with a few-eV plasma target.

VII. CONCLUDING REMARKS

We have presented a thorough investigation of the interaction of energetic ions with a nearly fully ionized hy-

drogen plasma. Every aspect, theoretical, numerical, and experimental has been given due attention. We have demonstrated that the most economical extension of the standard BBB theory for cold-matter stopping could be conveniently adapted to plasma targets (Sec. III).

Enhanced plasma stopping has been shown to arise from a contribution of the more flexible response of free electrons to incoming projectiles, with their larger effective charge Z_{eff} , due to a suppression of inflight ion-electron recombination in plasma. Those features are coherently included within the standard stopping model.

Conditions for a meaningful experimental verification of the SSM predictions have been discussed. They allow us to make use of standard available hardware such as dense discharges and linear accelerator (Sec. IV), provided the beam-plasma interface is suitably designed. Hydrogen discharges have been identified as a particularly convenient target, allowing a clean measurement of EPS, in a plasma essentially consisting of free electrons and protons (Sec. V). Specific characteristics of ion beam transmission through the target (Sec. VIA) have been disclosed. Finally, we have demonstrated a pretty good agreement between measured and SSM-estimated energy losses (Sec. VIB). In particular, their quasilinear dependence with respect to target density stresses the increasing reliability of the SSM approach for a nearly fully ionized. The Bethe term [Eq. (3.1)] increases by a factor of 2, while the Barkas term vanishes and the Bloch term remains nearly stationary when one compares plasma to cold-gas stopping.

In summary, we have provided quantitative evidence for the enhanced plasma stopping of energetic and multicharged ions, in agreement with the theoretically expected extension to plasmas [Eq. (3.1)] of the standard stopping formula (Bethe). Those results are of obvious interest for heavy-ion-driven fusion. They should allow us to increase significantly the quantitative understanding of the driver-pellet interaction near the end of the range, where the inner pellet hydrodynamical motion takes place.

ACKNOWLEDGMENT

GREMI and LPGP are "Unités de Recherche Associées au Centre National de la Recherche Scientifique."

- [1] R. O. Bangerter, J. W. K. Mark, and A. R. Thiessen, *Phys. Lett.* **88A**, 225 (1982); R. O. Bangerter, *Fus. Technol.* **13**, 348 (1988); F. C. Young, D. Mosher, S. J. Stephanakis, and S. A. Goldstein, *Phys. Rev. Lett.* **49**, 549 (1982); J. R. Roth, *Introduction to Fusion Energy* (Ibis, New York, 1986), p. 173; M. Jändel *et al.*, *Phys. Rev. A* **40**, 2799 (1989).
- [2] C. Deutsch, *Ann. Phys. (Paris)* **11**, (1986); *Laser Part. Beam* **2**, 449 (1984); see also R. C. Arnold and J. Meyer-

- Ter-Vehn, *Rep. Prog. Phys.* **50**, 559 (1987).
- [3] T. A. Mehlhorn, *J. Appl. Phys.* **52**, 6522 (1981); E. Nardi, E. Peleg, and Z. Zinamon, *Appl. Phys. Lett.* **39**, 46 (1981); G. Maynard and C. Deutsch, *Phys. Rev. A* **26**, 665 (1982); **27**, 574 (1983); C. Deutsch, G. Maynard, and H. Minoo, *J. Phys. (Paris) Colloq.* **44**, C8-67 (1983).
- [4] J. Meyer-Ter-Vehn, S. Witkowski, R. Bock, D. H. H. Hofmann, I. Hofmann, R. W. Müller, R. Arnold, and P. Mulser, *Phys. Fluids B* **2**, 1313 (1990).

- [5] D. W. Hewett, W. L. Kruer, and R. O. Bangerter, *Nucl. Fus.* **31**, 431 (1991); see also C. Deutsch, P. Fromy, X. Garbet, and G. Maynard, *Fus. Technol.* **13**, 362 (1988).
- [6] E. Nardi and Z. Zinamon, *Phys. Rev. Lett.* **49**, 1251 (1982); see also D. Bailey, Y. T. Lee, and R. M. More, *J. Phys. (Paris) Colloq.* **44**, C8-149 (1983).
- [7] C. Deutsch, G. Maynard, R. Bimbot, D. Gardes, S. Della-Negra, M. Dumail, B. Kubica, A. Richard, M. F. Rivet, A. Servajean, C. Fleurier, A. Sanba, D. H. H. Hoffmann, K. Weyrich, and H. Wahl, *Nucl. Instrum Methods A* **278**, 38 (1989).
- [8] G. Maynard and C. Deutsch, *J. Phys. (Paris) Colloq.* **49**, C7-151 (1988).
- [9] R. Bimbot, S. Della-Negra, D. Gardes, M. F. Rivet, C. Fleurier, B. Dumax, D. H. H. Hoffman, K. Weyrich, C. Deutsch, and G. Maynard, *Laser Int. Rel. Plasma Ph.* **8**, 665 (1988).
- [10] D. Gardes, R. Bimbot, S. Della Negra, M. Dumail, B. Kubica, A. Richard, M. F. Rivet, A. Servajean, C. Fleurier, A. Sanba, C. Deutsch, G. Maynard, D. H. H. Hoffman, K. Weyrich, and H. Wahl, *Europhys. Lett.* **8**, 701 (1988).
- [11] D. H. H. Hoffman, K. Weyrich, H. Wahl, Th. Peter, J. Meyer-Ter-Vehn, J. Jacoby, R. Bimbot, D. Gardes, M. F. Rivet, M. D. Dumail, C. Fleurier, A. Sanba, C. Deutsch, G. Maynard, R. Noll, R. Hass, R. Arnold, and S. Maurmann, *Z. Phys. A* **30**, 339 (1988).
- [12] D. H. H. Hoffman, K. Weyrich, H. Wahl, D. Gardes, R. B. Bimbot, and C. Fleurier, *Phys. Rev. A* **42**, 2313 (1990).
- [13] D. Gardes, R. Bimbot, M. F. Rivet, A. Servajean, C. Fleurier, D. Hong, C. Deutsch, and G. Maynard, *Laser Part. Beam* **8**, 575 (1990).
- [14] C. Fleurier, J. Mathias, B. Dumax, J. Pellicer, A. Bonnet, D. Gardes and B. Kubica, *Nucl. Instrum. Methods B* **61**, 236 (1991).
- [15] C. Deutsch, G. Maynard, R. Bimbot, D. Gardes, M. Dumail, B. Kubica, and A. Richard, M. F. Rivet, A. Servajean, C. Fleurier, D. Hong, D. A. Hoffmann, K. Weyrich, and H. Waal, *Laser Int. Rel. Plasma. Ph.* **9**, 593 (1991).
- [16] A. Servajean, Ph.D thesis, University of Orsay, 1990 (unpublished); also IPNO Report No. NT-9006, 1990 (unpublished).
- [17] D. Hong, Ph.D. thesis, University of Orléans, 1991 (unpublished).
- [18] G. Maynard (private communication).
- [19] V. Nikolaev, *Zh. Exsp. Teor. Fiz.* **51**, 1263 (1966) [*Sov. Phys. JETP* **24**, 847 (1967)].

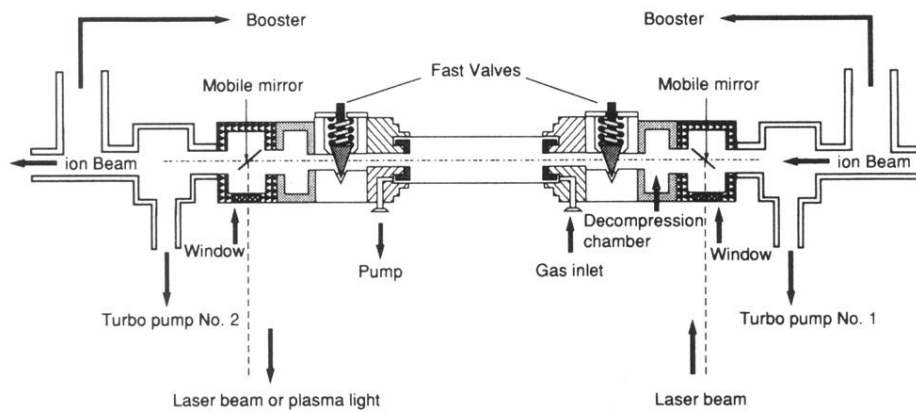


FIG. 6. Experimental setup. A linear plasma column is confined in an alumina tube connected to the beam line with two fast valves. Plasma diagnostics are realized using a laser beam injected during the plasma shot via two removable mirror systems.